Journal of Power Sources 206 (2012) 111–118

Contents lists available at SciVerse ScienceDirect

Journal of Power Sources

journal homepage: www.elsevier.com/locate/jpowsour

Fabrication and characterization of a $Sm_{0.2}Ce_{0.8}O_{1.9}$ electrolyte film by the spin-coating method for a low-temperature anode-supported solid oxide fuel cells

Rung-Je Yang, Maw-Chwain Lee*, Jen-Chen Chang, Tai-Nan Lin, Yang-Chuang Chang, Wei-Xin Kao, Lin-Song Lee, Shih-Wei Cheng

Chemical Engineering Division, Institute of Nuclear Energy Research, No. 1000, Wunhua Rd., Longtan Township, Taoyuan County 32546, Taiwan, ROC

ARTICLE INFO

Article history:
Received 28 November 2011
Accepted 1 January 2012
Available online 31 January 2012

Keywords:
Glycine nitrate combustion process
Samarium doped ceria ($Sm_{0.2}Ce_{0.8}O_{1.9}$)
Low-temperature solid oxide fuel cell
Spin-coating process
Membrane electrode assembly

ABSTRACT

Dense electrolyte films ~15 μm thick made of samarium-doped ceria (SDC) are fabricated by spin-coating. The SDC powders are synthesized by the glycine nitrate combustion process. It is found that nanoscale SDC powders can be obtained at 1000 °C. Cells constructed with an SDC electrolyte, a NiO + SDC composite anode, and an SSC–SDC/SSC bi-layer cathode are fabricated and tested at temperatures from 400 to 650 °C. SEM micrographs show that the SDC electrolyte layer adheres well to the porous anode and the cathode. The maximum power densities of the cell are 38, 84, 185, 303, 438, and 549 mW cm^{-2} at 400, 450, 500, 550, 600, and 650 °C, respectively. Analysis of the impedance spectra indicates that the electrode polarization dominates the total cell resistance at temperatures below 550 °C, and the ohmic resistance dominates the total cell resistance above 550 °C. The activation energies of the resistances show that the cell performance is significantly controlled by the electrode polarization resistance. Durability tests are performed over 950 h and indicate that the power density and the voltage gradually degrade with time at a rate of ~0.03 mW cm^{-2} h^{-1} and ~0.07 mV h^{-1}, respectively. Hence, a low-temperature solid oxide fuel cell has been developed.

1. Introduction

Solid oxide fuel cells (SOFCs), which are well recognized as environmentally friendly, highly efficient devices, and alternatives to conventional energy conversion systems, are considered to be one of the most important power generation technologies of the future [1]. A typical membrane electrode assembly (MEA) for SOFCs consists of two electrodes (an anode and a cathode) separated by an electrolyte. Yttrium-stabilized zirconia (YSZ) is considered to be one of the most reliable candidates for the electrolyte and has been widely used. However, for the YSZ to achieve sufficiently high oxygen-ion conductivity, a high operating temperature (up to 1000 °C) is required. The high operating temperature of traditional SOFCs with YSZ electrolytes results in high costs as well as problems with materials selection and degradation, such as electrode sintering or interfacial diffusion between the electrolyte and the electrode. Therefore, the development of low-temperature SOFCs (LT-SOFCs (400–600 °C)) is critical for cost reduction, long-term performance stability, and materials selection. To reduce the operating temperature, two approaches are widely applied to lower the resistance of the dense electrolyte membranes, including decreasing the thickness of the traditional YSZ electrolyte or using alternative materials with higher ionic conductivities at low temperatures [2–4]. Doped ceria has attracted much attention in recent years, especially as a possible solid electrolyte substitute for YSZ. The oxygen-ion conductivities of ceria-based electrolytes doped with various ions (e.g., Sr^{2+}, Ca^{2+}, Y^{3+}, La^{3+}, Gd^{3+}, and Sm^{3+}) at different concentrations have been extensively studied [5–8]. Their superior oxygen ionic conductivity [9] and good compatibility with electrodes allow the related SOFCs to have lower operating temperatures (from 1000 °C down to 600–800 °C). Among them, Gd^{3+} and Sm^{3+}-doped CeO_2 (GDC and SDC) are found to exhibit excellent oxygen-ion conductivity at specific doping levels due to the small enthalpy of association between the dopant cations and oxygen vacancies in the fluorite structure [10,11].

The performance of SOFCs can be significantly influenced by the microstructure of their electrolytes. A high densification of the sintering elements is required for a material to act as an electrolyte. The powder precursors are believed to have a great effect on the densification process, including the sintering temperature. Nanoscale particles tend to show better sintering ability than larger particles. Therefore, ceramics with a high sintering density might be obtained at lower temperatures (<1600 °C) when precursor powders having nanoscale characteristics are used. Low temperature

* Corresponding author. Tel.: +886 3 4711400x5930; fax: +886 3 4711411.
E-mail address: mclee@iner.gov.tw (M.-C. Lee).

0378-7753/$ – see front matter © 2012 Elsevier B.V. All rights reserved.
doi:10.1016/j.jpowsour.2012.01.024

processing is considered critical for energy-saving and cost reduction. In general, the characteristics of powders depend on the fabrication methods. The solid state reaction method has generally been employed for the fabrication of CeO_2-based powders for SOFC components [12]. In general, this process requires long distances for diffusion of the metal ions during synthesis accompanied by prolonged calcination at high temperatures. Therefore, powders synthesized by the solid state reaction method usually yield undesirable properties, including large particle size, inhomogeneity, and poor sinterability. To overcome these drawbacks, various methods, including sol–gel [13], co-precipitation [14,15], hydrothermal [16,17], thermal evaporation synthesis [18], and combustion methods [19], have been adopted for the preparation of nano-crystalline electrolyte materials in the literature.

Preparation of dense electrolyte films on porous electrodes or substrates is the critical step in the fabrication of high-performance solid-state fuel cells. Over the past few years, considerable efforts have been devoted to the development of intermediate-temperature SOFCs (IT-SOFCs (600–800 °C)) based on thin-film electrolytes of doped ceria [15,20–31]. Key processes employed to prepare these thin-film electrolytes on porous substrates can be classified into three categories. The first of these categories includes vapor-phase deposition methods, such as spray pyrolysis and pulsed laser deposition [20]. The second category includes liquid-phase deposition methods, such as spin coating, sol–gel, and the liquid-state deposition method [21,22]. The third category includes thin film techniques for the chemical engineering process with particle deposition/consolidation methods, such as dry pressing [15,23,24], tape casting [25], screen printing [26–28], and slurry spin coating [29–31]. Vapor-phase deposition methods have a high potential for the preparation of thin electrolytes with nano/micron-scale thickness, but have a major disadvantage with the associated high equipment and/or processing costs. With liquid-phase deposition techniques, especially with the spin coating of a precursor, compositional homogeneity at the molecular level can be achieved with a precursor solution rather than a prefabricated powder. This process favors the fabrication of an extremely thin ceramic film and is also relatively inexpensive in terms of equipment and processing costs. However, the particle deposition/consolidation methods are more popular and inexpensive compared with solution processing methods.

Ding et al. [15] successfully fabricated SOFC-MEAs consisting of thin film $Sm_{0.2}Ce_{0.8}O_{1.9}$ electrolytes with thicknesses of ~70 μm by the dry pressing method and demonstrated that the maximum power densities were 144 and 400 mW cm^{-2} at 500 and 600 °C, respectively. Cells consisted of a Ni–SDC anode and a $Sm_{0.5}Sr_{0.5}CoO_3$ (SSC)-SDC cathode. Misono et al. [25] used a multilayer tape casting technique to fabricate fuel cells consisting of a 20-μm SDC electrolyte, a Ni–SDC anode and a $La_{0.6}Sr_{0.4}Co_{0.2}Fe_{0.8}O_3$ cathode. The cell generated maximum power densities of 230 and 910 mW cm^{-2} at 500 and 650 °C, respectively. Xia et al. [26] adopted a screen-printing method to prepare a unit cell consisting of an SDC electrolyte film with a thickness of 30 μm and demonstrated maximum power densities of 188 and 397 mW cm^{-2} at 500 and 600 °C, respectively, for cells assembled with a Ni–SDC anode and a SSC–SDC cathode. Ai et al. [30] applied the spin-coating method to fabricate an anode-supported single cell that consisted of a 15 μm SDC electrolyte, a Ni–SDC anode and a $Ba_{0.5}Sr_{0.5}Co_{0.8}Fe_{0.2}O_{3-\delta}$–SDC cathode. The cells exhibited maximum power densities of 225 and 869 mW cm^{-2} at 500 and 650 °C, respectively. However, it is difficult to fabricate a thin SDC electrolyte film with a dense structure if the properties of the doped ceria powder are not properly controlled. One reason for this is that the CeO_2-based materials are difficult to densify when sintered at high temperatures (1600 °C) for long periods of time [32]. To reduce the sintering temperatures, powders with nanoscale particles are required. In this study, nanoscale $Sm_{0.2}Ce_{0.8}O_{1.9}$ powders were prepared by the glycine nitrate combustion process. The SDC powders were used as raw materials for the fabrication of electrolyte thin films in anode-supported fuel cells. Recently, spin coating processes have been developed and adopted for the fabrication of electrolytes for anode-supported SOFCs using prefabricated powders as the starting materials rather than using a precursor; this technique is referred to as slurry spin coating. Organic solvents are typically used in the slurry spin coating process [29–31], and these tend to be more expensive and harmful to the environment than using water as the solvent. A spin-coating process using water as the solvent has been adopted for the preparation of the SDC electrolyte thin film layer as a simple and effective process to fabricate thin and dense electrolyte films on porous substrates. The characteristics of the cell can be obtained by performance testing and the analysis of electrochemical impedance spectroscopy (EIS). Moreover, durability tests for the cells were performed with a constant current density at 650 °C.

2. Experimental

2.1. SDC powder preparations

$Sm_{0.2}Ce_{0.8}O_{1.9}$ powders and SSC powders were synthesized by a glycine nitrate combustion process (GNCP). The detailed fabrication procedures of the SDC and the SSC powders are described as follows, as reported by Chang et al. [33]. Stoichiometric amounts of $Sm(NO_3)_3{\cdot}6H_2O$ (99.9%, Strem chemicals, USA) and $Ce(NO_3)_2{\cdot}6H_2O$ (>98.5%, Merck chemicals, Germany) were used as the starting materials and dissolved in distilled water to form an aqueous solution. Glycine (NH_2—CH_2—COOH, >99.7%, Merck chemicals, Germany) was then added to the solution. The molar ratio of the glycine to the total metals was set at 1.6 according to the report of Peng et al. [19]. The solution was heated on a hot plate while stirring, converted to a viscous gel due to evaporation, and then the gel was swelled and subjected to a self-sustaining combustion. The as-prepared powder was then heated in the temperature range from 800 to 1200 °C for 2 h to form calcined samples with different crystallite sizes and microstructures. Powders calcined at 1000 °C were used to prepare the SDC slurry for spin coating.

2.2. Fabrication of the MEA

First, the NiO–SDC anode substrates were prepared by a uniaxial press with 55 MPa using a mixture of NiO and SDC powders. The NiO and SDC powders were obtained from All Achemie Ltd. (NiO, 99.9%, 325 mesh, USA) and Fuel Cell materials Ltd. (SDC20-HP, USA), respectively. The NiO and SDC powders were weighed (65:35 wt% ratio) and homogenized by ball milling using 5 mm YSZ balls in alcohol (99.5%) for 24 h. The anode powder was dried in an oven prior to use. The green NiO–SDC substrates (41 mm × 41 mm) were fabricated and thermally treated at 900 °C for 3 h. The SDC electrolyte films were fabricated by spin coating (Cee 200, Brewer Science, Inc., USA). A well-dispersed suspension consisting of 30 wt% SDC nanocrystallites and D.I. water was prepared by a ball milling with a high-energy device (JBM-B035, Just Nanotech Co., Taiwan). The electrolyte/electrode half-cell was then co-fired at 1500 °C for 6 h to achieve a dense SDC film. Finally, the SSC–SDC composite cathode paste was prepared by mixing 70 wt% SSC and 30 wt% SDC powders, and the pure SSC paste was subsequently coated onto the SDC electrolyte by a screen printer (EKRA XPRT1, Germany) and then calcined at 1000 °C for 2 h. Cells of NiO–SDC/SDC/SSC–SDC/SSC were obtained with an effective cathode area of 12 cm^2.

2.3. Characterization

The thermal behavior of the SDC powders was examined by DTA/TG (DTA/TG, Linseis L81/1750, Germany), using an ignited alumina as the reference material. The heating rate was 10 °C min^{-1} up to a maximum temperature of 1450 °C in an air atmosphere. Powder XRD methods using Ni-filtered CuK_α radiation (Bruker, D8 advance, Netherlands) were employed to identify crystalline phases and for crystallite size measurement. For phase identification, 2θ = 80–20° with a scan rate of 4° min^{-1} was used. The mean crystallite sizes of $Sm_{0.2}Ce_{0.8}O_{1.9}$ were calculated by the XRD-Scherrer formula [34] and the reflection peak of (1 1 1) was applied (crystallite size = $0.9\lambda/B\cos\theta$, where λ = 1.5406 Å, B = the full width of the half maximum (FWHM) of the peak in radians, and θ = the Bragg angle). The scan rate was 0.5° min^{-1}. The instrument peak width was calibrated using a well-crystallized alumina powder. The specific surface area was measured using the conventional nitrogen adsorption technique (Brunauer–Emmett–Teller (BET)-N_2) (Micromeritics, ASPS 2020, USA). The degree of agglomeration in the powder systems was characterized by the agglomeration number [35]. The unit cell was tested with a two-probe method. A platinum paste was applied to the cathode as the current collector, followed by attaching a platinum wire to the anode as the current and the voltage lead. Air was used as an oxidant. Hydrogen was humidified and used as fuel. The flow rates for the fuel and the oxidant were 335 and 670 ml min^{-1}, respectively. The electrochemical characteristics, such as the open-circuit voltage (OCV) and current–voltage (I–V) measurements, as well as the impedance analysis, were performed on an SI 1287 and SI 1260 (Solartron Instruments, Hampshire, UK) in the temperature range of 400–650 °C. Electrochemical impedance spectroscopy measurements were carried out under open circuit voltage conditions in a frequency range of 10 mHz to 0.1 MHz. After determination of their electrochemical performances, the SDC crystallites and the cells were examined with a scanning electron microscope (FE-SEM, Hitachi S-4800, Japan) to evaluate their morphology and microstructure. The oxidation state of Ce in the electrolyte was determined by X-ray photoelectron spectroscopy (XPS, PHI Quantera SXM, USA). The raw data were converted and plotted through OriginPro 8.0 software. All peaks of the plot were fitted with a Gaussian–Lorentzian shape function to decompose overlapping peaks. Peak positions were assigned according to the literature values obtained for CeO_2 [36].

3. Results and discussion

3.1. Nanoscale $Sm_{0.2}Ce_{0.8}O_{1.9}$ powders

The DTA/TG curves of the as-prepared powders are shown in Fig. 1, which shows that there is a weight loss of approximately 6% from 30 to 900 °C and that no distinctly endothermic or exothermic peaks can be seen. It shows that none of the organic phase remained in the powders. Chick et al. [37] pointed out that the flame temperature of the combustion process can reach 1100–1400 °C. Under these conditions, not only can a great amount of the nitrate ions and the residual carbon produced by the combustion process be burned out, but the SDC crystallites can be directly synthesized. The XRD patterns of the as-prepared powders presented in Fig. 2(a) are supported by this argument. Fig. 2 shows the XRD patterns of the as-prepared powder and the samples calcined in the temperature range of 800–1200 °C for 2 h. These results demonstrate that the as-prepared powder exhibited a cubic fluorite structure. All of the characteristic diffraction peaks corresponding to $Sm_{0.2}Ce_{0.8}O_{1.9}$ (JCPDS Card No. 75-0158) were observed. Moreover, no crystalline phases corresponding to Sm_2O_3 were found at any temperature,

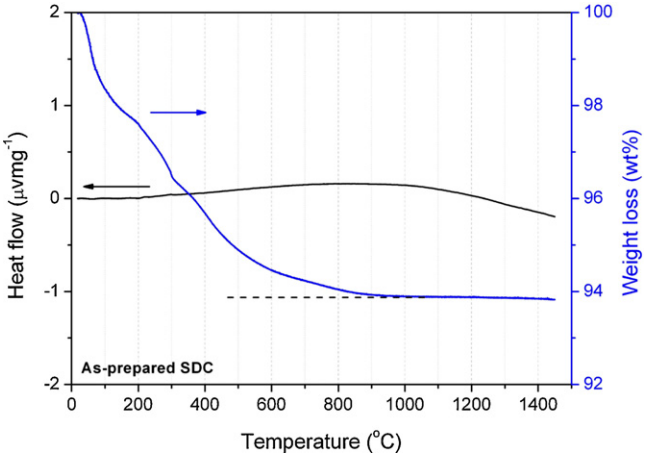

Fig. 1. The DTA/TG curves of the as-prepared powders with a heating rate of 10 °C min^{-1} in air.

which indicates that the SDC powder can be synthesized directly by the GNCP technique.

The physical properties of the as-prepared and calcined samples are summarized in Table 1. For sample AS, it shows that the crystallite size and the BET surface area are ~10 nm and ~39 m^2 g^{-1}, respectively. Furthermore, the results show that the crystallite sizes, as well as the specific surface areas, are significantly affected by the heating temperature. As the samples are thermally treated at temperatures of 800, 1000, and 1200 °C for 2 h, the BET surface areas decrease to values of ~25.59, ~13.65, and ~3.86 m^2 g^{-1}, respectively. The crystallite sizes of the SDC increase from 11 nm to ~41, ~48 and ~76 nm for the samples calcined at 800, 1000, and 1200 °C, respectively. When the heating temperature is greater than 1200 °C, the crystallites may grow to sizes larger than 100 nm.

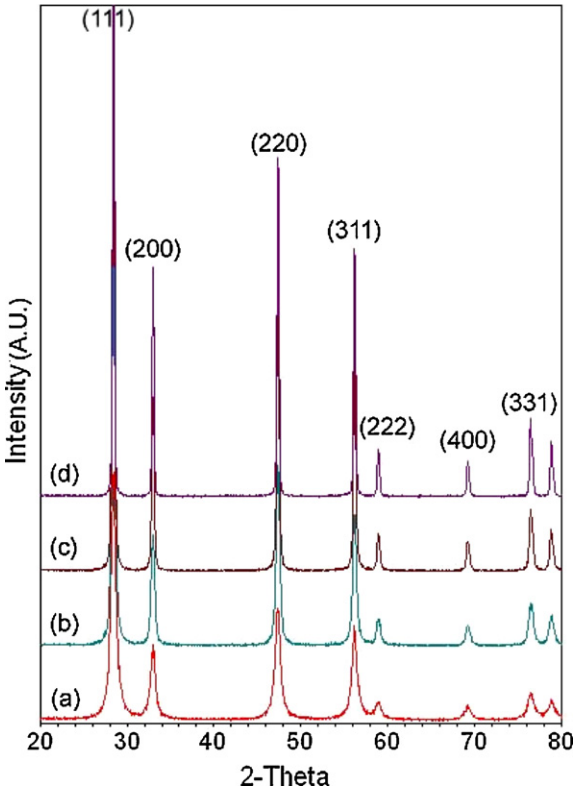

Fig. 2. XRD patterns of the (a) as-prepared powders and the samples calcined at (b) 800, (c) 1000, and (d) 1200 °C for 2 h.

Table 1
Physical properties of the as-prepared powders and the samples calcined at temperatures ranging from 800 to 1200 °C for 2 h.

Calcination temperature (°C)	Crystallite size (nm)[a]	BET surface area ($g\,m^{-2}$)	BET diameter (nm)[b]	Agglomeration number AN(50)[c]
As-prepared	11.2	38.61	21.7	7.32
800	22.0	25.59	32.8	3.32
900	41.5	14.67	57.2	2.62
1000	48.3	13.65	61.5	2.07
1100	56.0	7.24	115.9	8.88
1200	76.5	3.86	217.5	22.99

[a] XRD-Scherrer-formula on $(1\,1\,1)_{SDC}$.
[b] N_2-BET adsorption, $D = 6000/\rho S$, $\rho = 7.22\,g\,cm^{-3}$.
[c] $AN(50) = D^3_{BET}/D^3_{XRD}$.

The agglomeration number (AN(50)) derived from the ratio of the XRD crystallite size to the BET particle size gives an estimate of the average number of primary particles in each agglomerate [35]. It shows that the agglomeration number of the SDC powders decreases with increasing temperature for heating temperatures lower than 1000 °C. Fig. 3 shows the SEM micrographs of the as-prepared and the calcined samples. The as-prepared powders exhibit loose, highly porous structures and the agglomerated particles are linked together by weak forces. Peng et al. [19] pointed out that the porous structure and the weak bonds among the powders shown in Fig. 3(a) seemed to result from the great amount of gases released by the redox reaction. The porous structure of the powders

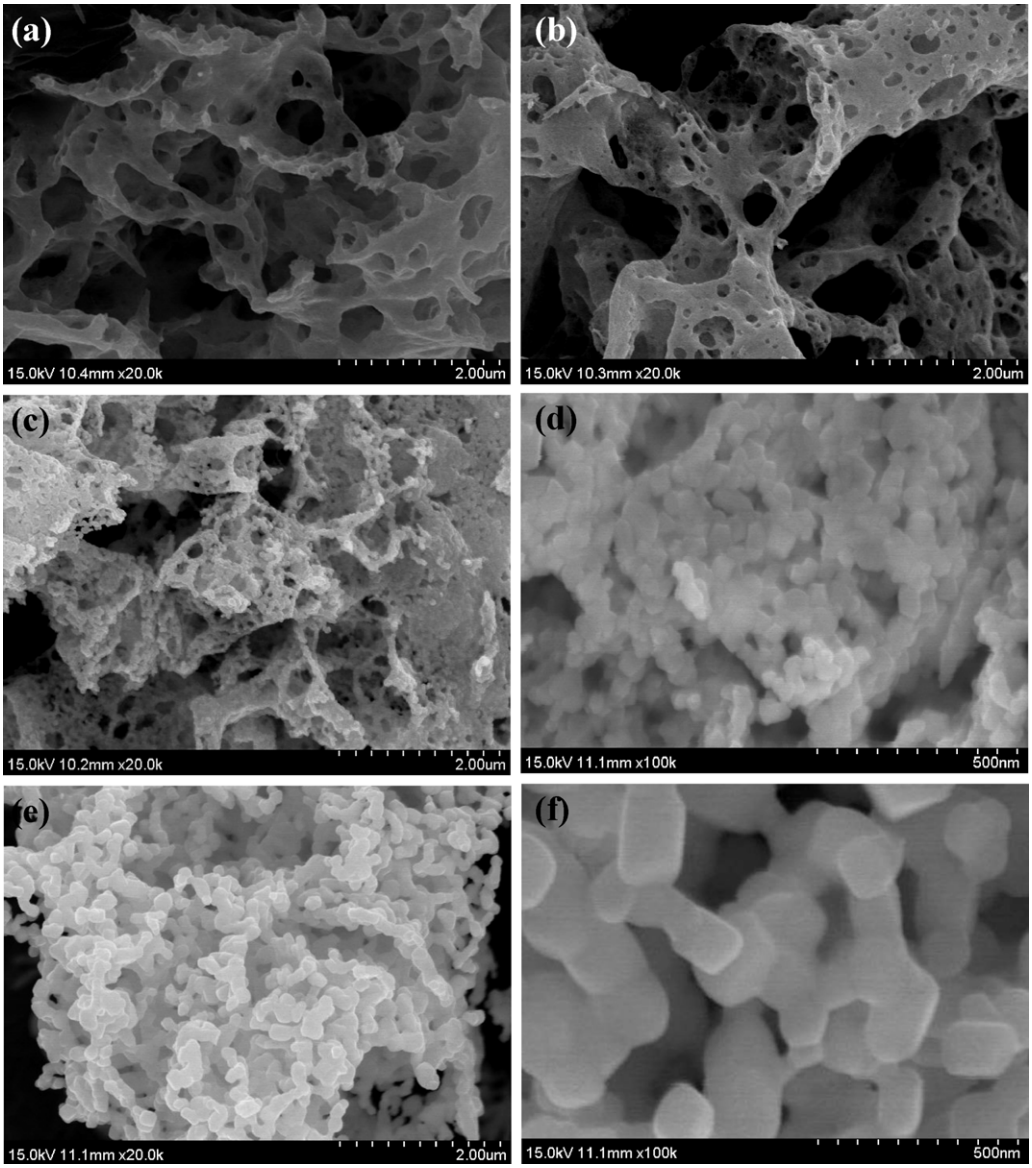

Fig. 3. SEM micrographs of the SDC powders of (a) as-prepared samples and samples calcined at (b) 800, (c, d) 1000, and (e, f) 1200 °C. The scale bars of (a, b, c, e) and (d, f) are 2 μm and 500 nm, respectively.

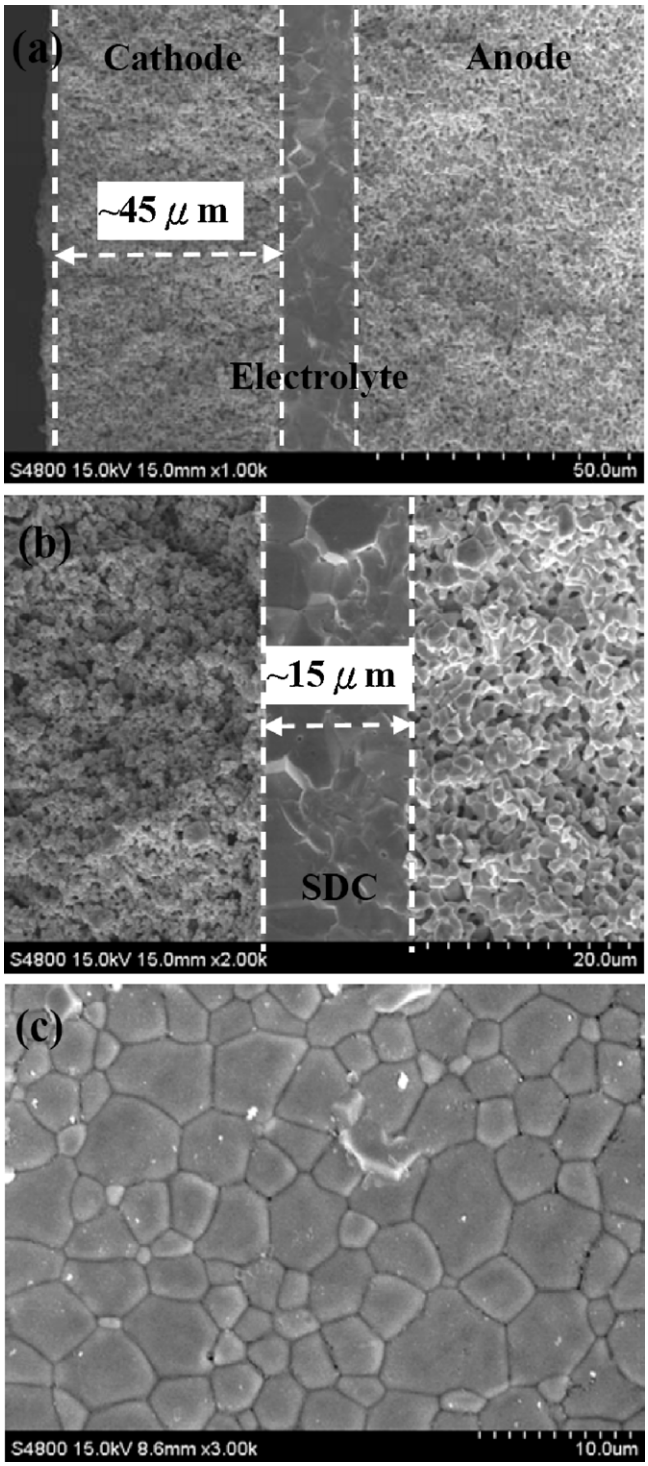

Fig. 4. SEM micrographs of the cross section of (a) an individual cell, (b) the dense SDC electrolyte, and (c) a top view of the SDC electrolyte film.

was retained and the crystallites grew to a size of ~50 nm when the temperatures were increased to 1000 °C (Fig. 3(c)). As the powders were thermally treated at 1200 °C, the sintering occurred and the particles formed necked structures (Fig. 3(f)). Fig. 3(d) and (f) indicate that the powders treated at 1000 °C exhibit crystallites with smaller sizes and lower degrees of agglomeration than do the powders treated at 1200 °C. The nanoscale $Sm_{0.2}Ce_{0.8}O_{1.9}$ powders with lower degreed of agglomeration (D = ~50 nm, BET = ~13.65 $m^2\ g^{-1}$)

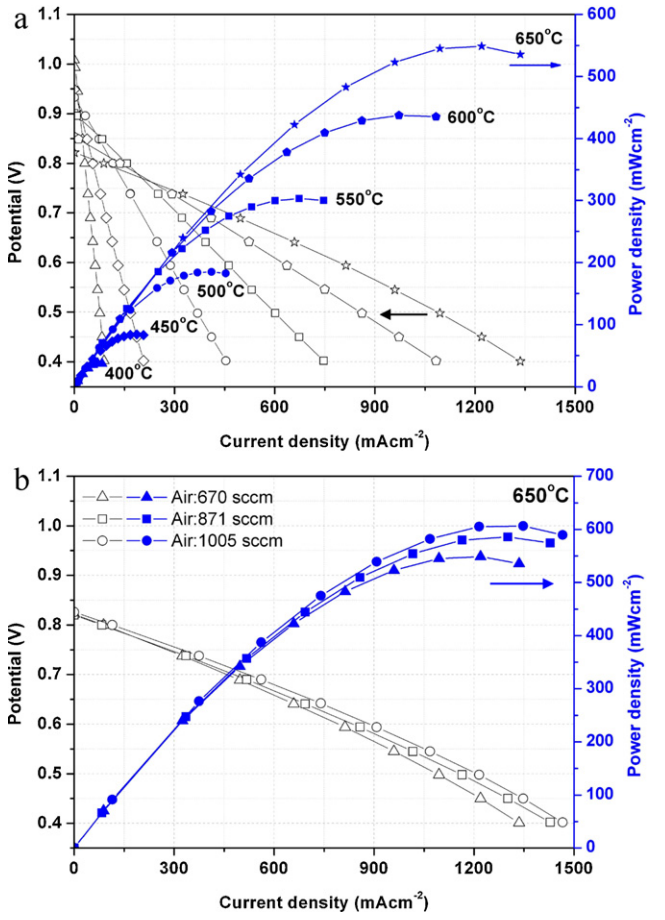

Fig. 5. *I–V* curves and the corresponding power densities for the cell with an SDC electrolyte (a) at temperatures from 400 to 650 °C, and (b) under different air flow rates at 650 °C.

can be obtained using the glycine nitrate combustion process accompanied by a subsequent heat treatment at 1000 °C.

3.2. Structure of the fabricated anode-supported solid oxide fuel cell

Fig. 4 shows SEM micrographs of a cross section (Fig. 4(a) and (b)) and of the SDC surface microstructures (Fig. 4(c)) of

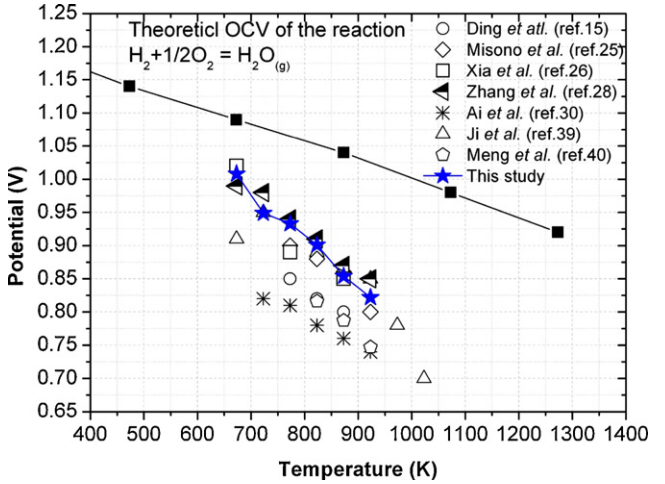

Fig. 6. Variations in the OCVs of the unit cells with an SDC electrolyte at different temperatures as reported in previous studies and obtained in this study.

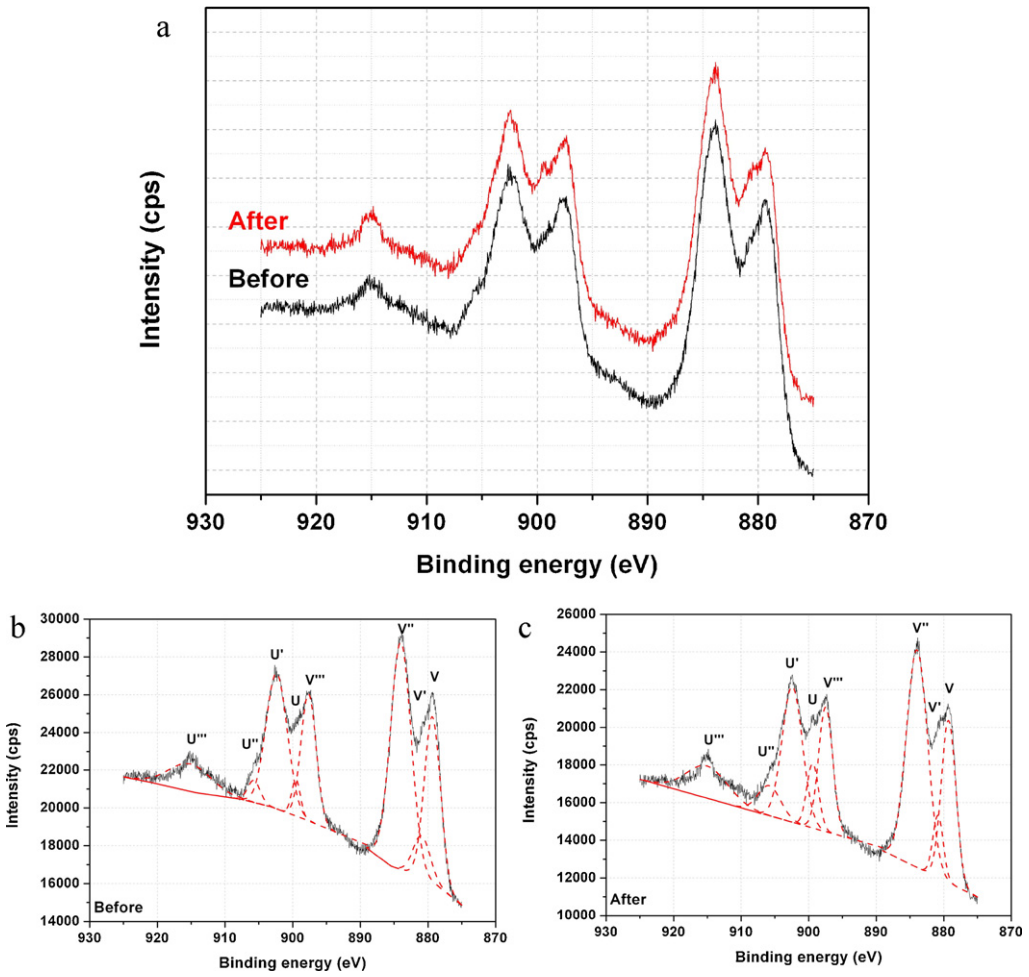

Fig. 7. (a) The Ce 3d spectra of the electrolyte before and after cell performance analysis, (b), (c) the fitting results of the spectra before and after cell performance, respectively. Solid lines represent the experimental spectra and the dashed lines are for the results with peak fitting. u''', u'', u, v''', v'', and v were characterized by Ce^{4+} ions, and the u' and v' were characterized by Ce^{3+}.

the anode-supported cell. The cell consists of layers of a porous Ni–SDC anode ~900 μm thick, a dense SDC electrolyte ~15 μm thick, and a porous SSC–SDC/SSC bi-layer cathode ~45 μm thick. It is observed that the SDC electrolyte layer adhered well to the porous Ni–SDC anode and the SSC–SDC/SSC cathode. The dense structure of the electrolyte layer is clearly shown in Fig. 4(b). Furthermore, as shown in Fig. 4(b) and (c), the SDC layer is very dense except for a few isolated pores. Moreover, no cross-layer pinholes or cracks are observed.

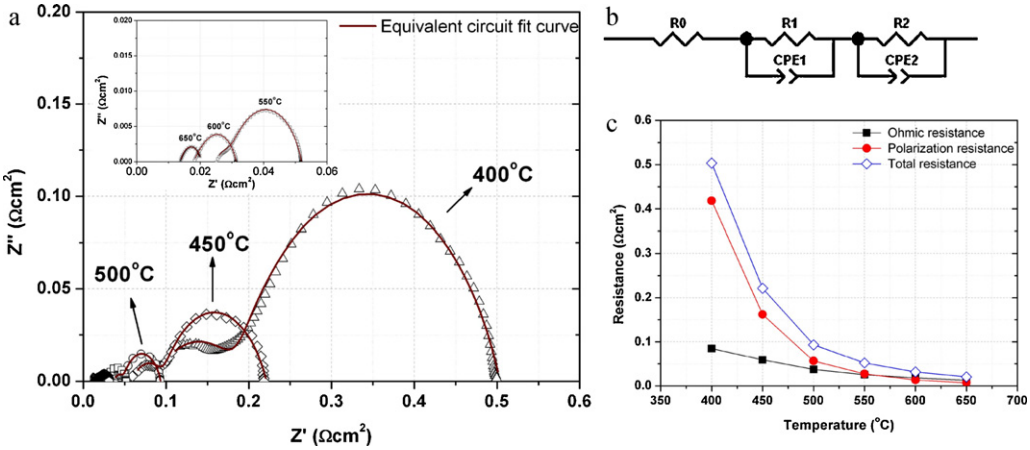

Fig. 8. (a) The impedance spectra of the cell, (b) the equivalent circuit, and (c) the variations in the ohmic and the total electrode polarization resistances measured at different temperatures.

Table 2
Fitting results for the impedance spectra and the electrochemical characteristics at different temperatures.

Temperature (°C)	Resistances (Ω cm^2)			Open-circuit voltage (V)	Maximum power density (mW cm^{-2})
	R_0	R_p	R_t		
400	0.085	0.418	0.503	1.008	38
450	0.059	0.162	0.221	0.949	84
500	0.037	0.056	0.093	0.933	185
550	0.025	0.027	0.052	0.901	303
600	0.018	0.013	0.031	0.854	438
650	0.013	0.007	0.020	0.822	549

3.3. Performance of the SOFC

The voltages and power densities of the cells as a function of current density at different temperatures are presented in Fig. 5, which shows that the cell voltage decreases approximately linearly with increasing current density. These results indicate that ohmic resistance is primarily responsible for the reduction in the cell voltage. The open-circuit voltages (OCVs) are 1.008, 0.949, 0.933, 0.901, 0.854, and 0.822 V, and the maximum power densities of the cells are 38, 84, 185, 303, 438, and 549 mW cm^{-2} at 400, 450, 500, 550, 600, and 650 °C, respectively. Furthermore, the maximum power density achieved 608 mW cm^{-2} at 650 °C by the increase in feed rate of air. In this work, the OCV values show a large discrepancy from the theoretical values for H_2–O_2 fuel cells, i.e., 1.07 V at 500 °C. Variations in the OCV of the unit cells with the SDC electrolyte at different temperatures have been reported in previous studies [15,25,26,28,30,39–40] and are summarized in Fig. 6 along with the results obtained in this study. The difference between the measured values of the OCVs and the theoretical values increases with increasing operating temperature. This increase can be attributed to a problem with increasing electronic conductivity of the doped ceria materials in atmospheres that promote reduction processes [38]. The issue lies in the oxidation states of Ce^{3+}/Ce^{4+}, and the primary results show that the ratio of Ce^{3+}/Ce^{4+} in the electrolytes are 0.262 and 0.295 before and after cell performance analysis, respectively (Fig. 7). In addition, the performance of individual cells increases with increasing operating temperature, which indicates that the electrolyte (or ohmic) resistance and the interfacial (or electrode) polarization decrease with increasing operating temperature due to enhancements in the oxygen ionic conductivity and the catalytic activity. The performance of the cells examined at temperatures ranging from 500 to 600 °C is higher than values that have been previously reported [15,26,41]. The maximum power densities of the cells with SSC composite cathodes and SDC electrolytes reported by Xia et al. [26], Yin et al. [41], and Ding et al. [15] are 240, 180, and, 253 mW cm^{-2} at 550 °C, respectively.

Fig. 8(a) and (b) shows the cell impedance spectra at different temperatures under open-circuit conditions and the equivalent circuit, respectively. The impedance spectra are characterized by a large arc at low frequencies and a much smaller one at high frequencies. This indicates that a molecular oxidation–reduction is controlled by at least two different electrode processes. In the equivalent circuit, R_0 corresponds to the total ohmic resistance including the electrolyte, electrodes and connection wires. The resistance R_1 is the charge-transfer resistance, which is attributed to the interfacial resistance between the electrodes and the electrolyte. The resistance R_2 is the non-charge-transfer process contributed by the oxygen surface exchange, catalytic reactions, solid-state diffusion, and gas-phase diffusion inside and outside the electrode [39]. The CPE_1 and CEP_2 are constant phase elements.

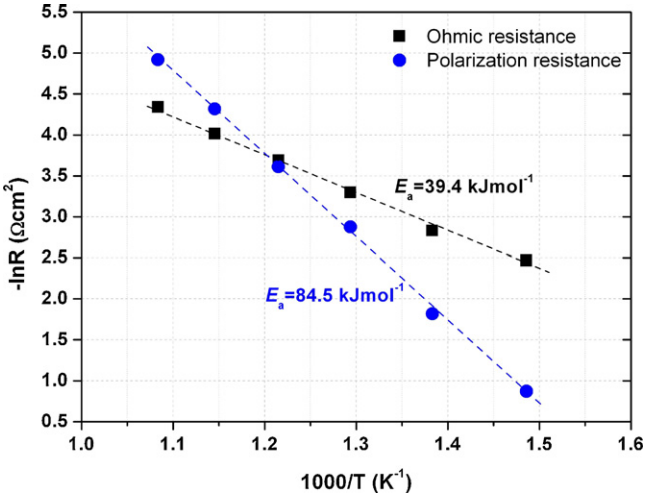

Fig. 9. Arrhenius plots of the ohmic and total electrode polarization resistances measured at different temperatures.

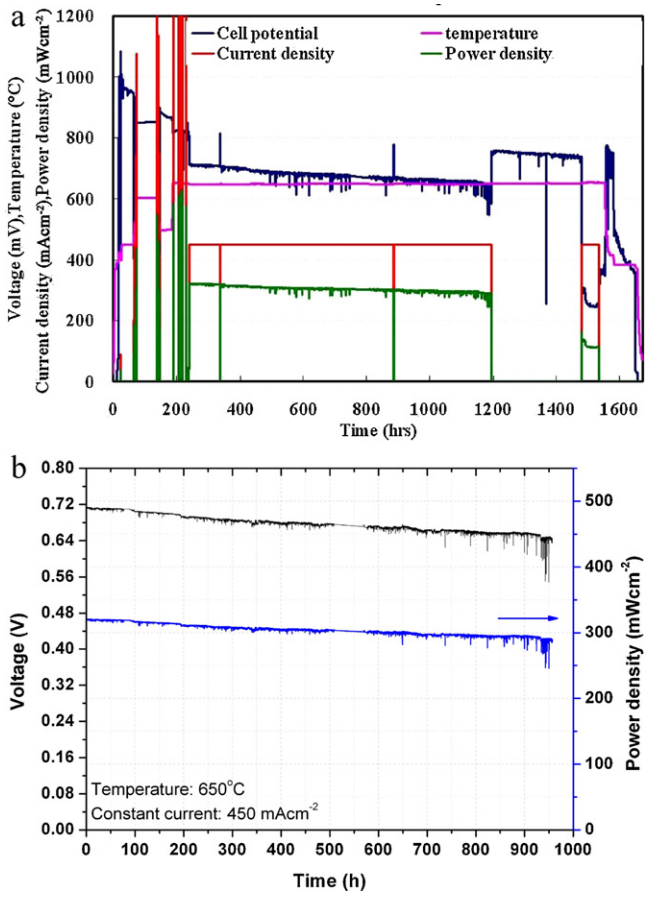

Fig. 10. (a) The entire cell testing process and (b) the durability test of the cell performance (the active area = 12 cm^2, H_2 = 335 cc min^{-1} and air = 670 cc min^{-1}).

The fitting results of the impedance spectra (solid lines) and the electrochemical characteristics (symbols) are presented in Fig. 8(a) and summarized in Table 2. The total ohmic resistance (R_0), total electrode polarization resistance ($R_p = R_1 + R_2$) and total resistances ($R_t = R_0 + R_p$) of the cell determined from the impedance spectra are shown in Fig. 8(c). This figure shows that all of the resistances decrease with increasing temperature. The electrode polarization dominates the total cell resistance at temperatures below 550 °C. With an increase in temperature, the ratio of the electrode polarization to the total cell resistance decreases rapidly (83–52%), and the effect of the ohmic resistance on the total cell resistance is relatively increased (17–48%). Therefore, the performance of the cell is significantly limited by the ohmic resistance at high temperatures (>550 °C). Fig. 9 shows Arrhenius plots of the ohmic resistance and the total electrode polarization resistance of the cell. It shows that the activation energies (E_a) of the ohmic resistance and the total electrode polarization resistance are 39.4, and 84.5 kJ mol^{-1}, respectively. These results show that the E_a of the polarization resistance is larger than that of the ohmic resistance, indicating that the role of the polarization resistance might be critical for the overall cell performance. The cell performance tests and the durability tests were examined over 1600 and 950 h, respectively, as shown in Fig. 10(a) and (b). The durability tests of the cells were carried out under a constant current density of 450 mA cm^{-2} at 650 °C. The cells were tested for 240 h to obtain the performance data. During the durability test, the power density and the voltage gradually degraded with time at a rate of ~0.03 mW cm^{-2} h^{-1} and ~0.07 mV h^{-1}, respectively. Further efforts must be put forth to achieve the targets of the low degradation rate and high durability that are required for commercial applications.

4. Conclusions

It is found that the $Sm_{0.2}Ce_{0.8}O_{1.9}$ powders with crystallite sizes of approximately 10 nm can be synthesized directly by the GNCP technique. With heating temperatures higher than 1200 °C, the crystallite size may grow to sizes larger than 100 nm. The nanoscale SDC powders with lower degrees of agglomeration (D = ~50 nm, BET = ~13.65 m^2 g^{-1}) can be obtained at 1000 °C. The SEM micrographs show that the SDC electrolyte layer adheres well to the porous Ni–SDC anode and the SSC–SDC/SDC bi-layer cathode to achieve good mechanical compatibility. The maximum power densities of the cells are 38, 84, 185, 303, 438, and 549 mW cm^{-2} at 400, 450, 500, 550, 600, and 650 °C, respectively. Furthermore, the maximum power density achieved 608 mW cm^{-2} at 650 °C by the increase in feed rate of air. The impedance spectra analysis indicates that electrode polarization dominates the total cell resistance at temperatures below 550 °C, and the effect of the ohmic resistance on the total cell resistance increases with increasing temperature. Furthermore, the E_a of the resistances shows that the cell performance is dominated by the electrode polarization resistance. The durability test examined over 950 h indicates that the power density and the voltage gradually degraded with time at a rate of ~0.03 mW cm^{-2} h^{-1} and ~0.07 mV h^{-1}, respectively. Hence, a LT-SOFC has been approximately developed, but the cell durability and the power density must be enhanced.

Acknowledgements

This work was supported by the National Nanotechnology Program (NNP) of the Taiwan Government. The administrative support from the Institute of Nuclear Energy Research is highly appreciated.

References

[1] Y. Jiang, A.V. Virkar, J. Electrochem. Soc. 148 (2001) A706–A709.
[2] B.C.H. Steele, Solid State Ionics 134 (2000) 3–20.
[3] S. Zha, C. Xia, X. Fang, H. Wang, D. Peng, G. Meng, Ceram. Int. 27 (2001) 649–654.
[4] S. Zha, Q. Fu, Y. Lang, C. Xia, G. Meng, Mater. Lett. 47 (2001) 351–355.
[5] D.Y. Wang, D.S. Park, J. Griffith, A.S. Nowick, Solid State Ionics 2 (1981) 95–105.
[6] G.B. Balazs, R.S. Glass, Solid State Ionics 76 (1995) 155–162.
[7] C. Tian, S.W. Chan, Solid State Ionics 134 (2000) 89–102.
[8] T.S. Zhang, P. Hing, H.T. Huang, J.A. Kilner, Solid State Ionics 148 (2002) 567–573.
[9] G.M. Christi, F.P.F. van Berkel, Solid State Ionics 83 (1996) 17–27.
[10] R. Gerhard-Anderson, A.S. Nowick, Solid State Ionics 5 (1981) 547–550.
[11] J.A. Kilner, Solid State Ionics 8 (1983) 201–207.
[12] Z. Zhan, T.-L. Wen, H. Tu, Z.-Y. Lu, J. Electrochem. Soc. 148 (5) (2001) A427–A432.
[13] W. Huang, P. Shuk, M. Greenblatt, Solid State Ionics 100 (1997) 23–27.
[14] H.B. Li, C.R. Xia, M.H. Zhu, Z.X. Zhou, G.Y. Meng, Acta Mater. 54 (2006) 721–727.
[15] D. Ding, B. Liu, Z. Zhu, S. Zhou, C. Xia, Solid State Ionics 179 (2008) 896–899.
[16] J.S. Lee, S.C. Choi, Mater. Lett. 58 (2004) 390–393.
[17] M.Y. Cheng, D.H. Hwang, H.S. Sheu, B.J. Hwang, J. Power Sources 175 (2008) 137–144.
[18] W. Bai, K.L. Choy, N.H.J. Stelzer, J. Schoonman, Solid State Ionics 116 (1999) 225–228.
[19] R. Peng, C. Xia, Q. Fu, G. Meng, D. Peng, Mater. Lett. 56 (2002) 1043–1047.
[20] D. Yang, X. Zhang, S. Nikumb, C. Decês-Petit, R. Hui, R. Maric, D. Ghosh, J. Power Sources 164 (2007) 182–188.
[21] S.G. Kim, S.P. Yoon, S.W. Nam, S.H. Hyun, S.A. Hong, J. Power Sources 110 (2002) 222–228.
[22] Y.Y. Chen, W.C.J. Wei, Solid State Ionics 177 (2006) 351–357.
[23] C. Xia, W. Rauch, F. Chen, M. Liu, Solid State Ionics 149 (2002) 11–19.
[24] Z. Gao, J. Huang, Z. Mao, C. Wang, Z. Liu, Int. J. Hydrogen Energy 35 (2010) 731–737.
[25] T. Misono, K. Murata, T. Fukui, J. Chaichanawong, K. Sato, H. Abe, M. Naito, J. Power Sources 175 (2006) 754–757.
[26] C. Xia, F. Chen, L. Liu, Electrochem. Solid-State Lett. 4 (5) (2001) A52–A54.
[27] R. Peng, C. Xia, D. Peng, G. Meng, Mater. Lett. 58 (2004) 604–608.
[28] X. Zhang, M. Robertson, S. Yick, C. Decês-Petit, E. Styles, W. Qu, Y. Xie, R. Hui, J. Roller, O. Kesler, R. Maric, D. Ghosh, J. Power Sources 160 (2006) 1211–1216.
[29] N. Ai, Z. Lü, K. Chen, X. Huang, Y. Liu, R. Wang, W. Su, J. Membr. Sci. 286 (2006) 255–259.
[30] N. Ai, Z. Lü, K. Chen, X. Huang, B. Wei, Y. Zhang, S. Li, X. Xin, X. Sha, W. Su, J. Power Sources 159 (2006) 637–640.
[31] R. Hui, Z. Wang, S. Yick, R. Maric, D. Ghosh, J. Power Sources 172 (2007) 840–844.
[32] T. Kudo, H. Obayashi, J. Electrochem. Soc. 122 (1) (1975) 142–1477.
[33] J.-C. Chang, M.-C. Lee, R.-J. Yang, Y.-C. Chang, T.-L. Lin, C.-H. Wang, W.-X. Kao, L.-S. Lee, J. Power Sources 196 (2011) 3129–3133.
[34] B.D. Cullity, Elements of X-ray Diffraction, 2nd ed., Addison-Wesley, London, 1978.
[35] B.C. Mutsuddy, R.G. Ford, Ceramic Injection Molding, Materials Technology Series, 1st ed., Chapman & Hall, New York, 1995.
[36] A.Q. Wang, P. Punchaipetch, R.M. Wallace, T.D. Golden, J. Vac. Sci. Technol. B21 (2003) 1169–1175.
[37] L.A. Chick, L.R. Pederson, G.D. Maupin, J.L. Bates, L.E. Thomas, G.J. Exarhos, Mater. Lett. 10 (1, 2) (1990) 6–12.
[38] L. Navarrok, F. Marques, J. Frade, J. Electrochem. Soc. 144 (1) (1997) 267–273.
[39] Y. Ji, J. Liu, T. He, L. Cong, J. Wang, W. Su, J. Alloys Compd. 353 (2003) 257–262.
[40] G. Meng, C. Jiang, J. Ma, Q. Ma, X. Liu, J. Power Sources 173 (2007) 189–193.
[41] Y. Yin, S. Li, C. Xia, G. Meng, Electrochim. Acta 51 (2006) 2594–2598.